

Direct evidence for charge compensation induced large magnetoresistance in thin WTe_2

Yaojia Wang^{||,†}, Lizheng Wang^{||,†}, Xiaowei Liu[†], Heng Wu[†], Pengfei Wang[†], Dayu Yan[‡], Bin Cheng[†], Youguo Shi[‡], Kenji Watanabe[§], Takashi Taniguchi[§], Shi-Jun Liang^{*,†}, Feng Miao^{*,†}

[†]National Laboratory of Solid State Microstructures, School of Physics, Collaborative Innovation Center of Advanced Microstructures, Nanjing University, Nanjing 210093, China.

[‡]Institute of Physics, Chinese Academy of Sciences, Beijing 100190, China

[§]National Institute for Materials Science, 1-1 Namiki Tsukuba, Ibaraki 305-0044, Japan

Abstract: Since the discovery of extremely large non-saturating magnetoresistance (MR) in WTe_2 , much effort has been devoted to understanding the underlying mechanism, which is still under debate. Here, we explicitly identify the dominant physical origin of the large non-saturating MR through *in-situ* tuning of the magneto-transport properties in thin WTe_2 film. With an electrostatic doping approach, we observed a non-monotonic gate dependence of the MR. The MR reaches a maximum (10600%) in thin WTe_2 film at certain gate voltage where electron and hole concentrations are balanced, indicating that the charge compensation is the dominant mechanism of the observed large MR. Besides, we show that the temperature dependent magnetoresistance exhibits similar tendency with the carrier mobility when the charge compensation is retained, revealing that distinct scattering mechanisms may be at play for the temperature dependence of magneto-transport properties. Our work would be helpful for understanding mechanism of the large MR in other nonmagnetic materials and offers an avenue for achieving large MR in the non-magnetic materials with electron-hole pockets.

Keywords: WTe_2 , large non-saturating magnetoresistance, charge compensation, *in-situ* tuning

As a layered non-magnetic material, WTe₂ exhibits an extremely large non-saturating magnetoresistance (MR)¹. This discovery has stimulated the observation of topological Weyl state²⁻⁴, superconductivity⁵⁻¹⁰, ferroelectricity¹¹ and quantum spin Hall state in WTe₂¹². Uncovering and identifying the physical origin of this unusually large MR is of crucial significance for devising novel magnetic sensor and nanostructure memory devices. So far, distinct physical mechanisms, such as electron-hole compensation¹³⁻¹⁵ and spin texture induced suppression of backscattering^{16, 17}, have been proposed to explain the physical origin. The charge compensation as the most studied mechanism has been supported by the observed nearly identical electron and hole pockets at Fermi surface by angle-resolved photoemission spectroscopy (ARPES)^{15, 18-20}. However, these ARPES experiments only offer an indirect evidence. The most desirable way to validate this mechanism is to study the magneto-transport property by *in-situ* tuning carrier density across the compensation point. By using some approaches such as high-pressure²¹, chemical^{22, 23} or electrostatic doping²⁴ to tune the carrier density, the observed reduction in the MR seems to be consistent with the charge compensation mechanism. Nevertheless, it is challenging to access the charge compensation point in these experiments due to sample degradation or narrow tuning range of the carrier density. Moreover, the variation of carrier mobility during tuning of the carrier density would affect the MR, as pointed out in many experiments in which the low mobility leads to small MR in thin films (*i.e.* less than 1000% in samples with thickness below 10 nm) and a reduction in the MR of bulk samples²⁵⁻³⁸. The entanglement of different factors in the study of MR makes it challenging to identify the intrinsic mechanism. Therefore, the physical origin of the large MR is still under debate and more effort is required to uncover it explicitly.

In this work, we performed a systematic study on *in-situ* tuning of the MR in WTe₂ thin film devices (about 10 nm) via an electrostatic doping approach. With hexagonal boron nitride (h-BN) as the protective and dielectric layer, the MR is tuned to exhibit dramatic change with non-monotonic gate dependence with peak value appearing at a certain voltage. Based on theoretical analysis, we demonstrate that the MR reaches the maximum value at the charge compensation point and decreases rapidly with carrier

concentration deviating from the compensation point. In addition, the achieved MR (10600%) at charge compensation is one to two orders of magnitude larger than previous reported values (100% ~ 1000% at 14 T) in thin films with similar thickness (~10 nm)^{24, 28-34, 36}. These results unambiguously identify the charge compensation effect as the dominant mechanism for the observed large MR in WTe₂ in an explicit manner. Furthermore, we show that the charge compensation can be retained within a wide temperature regime where the temperature dependence of the MR shows the similar tendency with carrier mobility, which enables us to reveal the charge scattering mechanisms for the temperature dependence of MR.

The WTe₂ devices covered with h-BN were fabricated in an inert atmosphere glove box to avoid quality degradation^{26, 33, 35, 39, 40}. Both WTe₂ thin films (about 10 nm) and h-BN films (about 20 nm) were first exfoliated onto SiO₂/Si substrate via mechanical exfoliation. We then picked up the h-BN and WTe₂ films successively and transferred them onto the pre-prepared Hall bar electrodes (Ti 5 nm/Au 30 nm) by using polypropylene carbon (PPC) films⁴¹. Few-layer graphene (FLG) flakes exfoliated on PDMS were finally transferred onto the h-BN films to act as top gate electrodes. Figure 1a shows the schematic cross-sectional structure and the optical image of a fabricated device. All electrical measurements in this work were performed using the conventional four-probe technique.

We first characterized the magneto-transport properties of a thin film device by measuring the temperature dependence of the longitudinal resistivity ($\rho(T)$) in different perpendicular magnetic fields, with results shown in Figure 1b. The sample shows metallic behavior at zero field. The ratio of residual resistivity ratio $\text{RRR} \equiv \rho(300 \text{ K})/\rho(2 \text{ K})$ is about 64, indicating the high quality of the h-BN protected thin film devices. At low temperature region ($1.6 \text{ K} < T < 15 \text{ K}$), the temperature dependence of zero field resistivity can be well described by $\rho_{xx}(T, 0) = \rho_0 + aT^2$ (as shown in the inset) manifesting electron-electron scattering at low temperatures in WTe₂⁴², where ρ_0 is the residue resistivity and a is a free parameter. With applying a magnetic field, $\rho_{xx}(T, B)$ curves present a transition from metallic-like state at high temperatures to insulator-like

state at low temperatures. This is similar to the turn-on behavior observed in bulk WTe₂⁴²⁻⁴⁴, suggesting the onset of large MR at low temperatures in our high-quality thin film devices. Such turn-on behavior is not the signal of field induced metal-insulator phase transition in WTe₂, but a manifestation of the MR behavior determined by the two-band theory. Figure 1c shows the MR measured at 1.6 K, where $\rho_{xx}(B)$ exhibits non-saturating increase with magnetic field and Shubnikov-de Haas (SDH) oscillations at high field. The MR(B) curve ($\text{MR}(B) = (\rho_{xx}(B) - \rho_0)/\rho_0 \times 100\%$) can be fitted by a power law of $\text{MR} \sim B^n$ with $n = 1.81$ (Inset of Figure 1c), close to the quadratic relation in bulk WTe₂^{42, 45, 46}.

By applying the electrostatic doping through h-BN film, we can continuously tune the magneto-transport properties of the thin WTe₂ film, which offers a direct way to reveal the physical origin of the large non-saturating MR. Figure 2(a) shows the gate voltage dependence of longitudinal resistivity measured with and without magnetic field at 1.6 K. Compared to the resistivity at zero field, the longitudinal resistivity at a finite magnetic field ($B = 12$ T) varies non-monotonously with gate voltage (V_{tg}) and reaches the maximum at certain V_{tg} . To gain further insight into the gate voltage dependence of the MR, we present the MR and the Hall resistivity at different gate voltages, as shown in Figure 2(b) and Figure 2(c) respectively. The MR curve exhibits a non-monotonic change with increasing gate voltage from -10 V to 6 V. The $\rho_{xy}(B)$ curves show a nonlinear feature, indicating the existence of two types of charge carriers in the device. At high field, the Hall resistivity changes dramatically with the gate voltage, and presents a sign change near the voltage of -6 V, which indicates the significant change of charge carriers.

The relation between the MR and charge carriers can be analyzed quantitatively by using the two-band theory⁴⁷, which can be described by:

$$\rho_{xx}(B) = \frac{(n_e\mu_e + n_h\mu_h) + (n_e\mu_h + n_h\mu_e)\mu_e\mu_h B^2}{e[(n_e\mu_e + n_h\mu_h)^2 + (n_h - n_e)^2\mu_e^2\mu_h^2 B^2]} \quad (1)$$

$$\rho_{xy}(B) = \frac{(n_h\mu_h^2 - n_e\mu_e^2)B + (n_h - n_e)\mu_e^2\mu_h^2 B^3}{e[(n_e\mu_e + n_h\mu_h)^2 + (n_h - n_e)^2\mu_e^2\mu_h^2 B^2]} \quad (2)$$

$$\text{MR}(B) = \frac{(n_e\mu_e + n_h\mu_h)^2 + \mu_e\mu_h(n_e\mu_e + n_h\mu_h)(n_h\mu_e + n_e\mu_h)B^2}{(n_e\mu_e + n_h\mu_h)^2 + (n_h - n_e)^2\mu_e^2\mu_h^2 B^2} - 1. \quad (3)$$

Where $n_e(n_h)$ is the electron (hole) density, $\mu_e(\mu_h)$ is the electron (hole) mobility, e is the

elementary charge. At each voltage, the $\text{MR}(B)$ and $\rho_{xy}(B)$ curves are fitted simultaneously by Eqs. (3) and (2), with fitting curves (dashed lines) plotted in Figure 2b and Figure 2c. The excellent agreement between the fitted curves and experimental data indicates that the two-band theory can be used to account for the varying behavior of MR. Thus, we can further extract the carriers' mobilities and densities at different gate voltages, with the results shown in Figure 2d and Figure 2e respectively. With increasing gate voltage, the electron mobility (μ_e) decreases but hole mobility (μ_h) increases (Figure 2d). The oppositely varying trends of electron and hole mobilities may originate from the surface scattering induced nonlocal effect³⁰. Applying a negative (positive) gate voltage would increase (reduce) the surface scattering of holes and lead to the reduction (increase) of the hole mobility, which has opposite effects on electrons. Changing the gate voltage from -10 V to 6 V also gives rise to an opposite variation in the electron (n_e) and hole densities (n_h). This is reasonable as applying a positive (negative) gate voltage will accumulate electrons (holes) in the thin film. It is noticeable that, with increasing gate voltage, a crossover occurs near -6 V, indicating the dominant carrier changes from hole to electron after passing this crossover point. This carrier type changing behavior is well consistent with the sign change of the Hall resistivity near $V_{\text{tg}} = -6$ V (Figure 2c), which can be interpreted by the two-band theory. According to Eq. (2), the sign of Hall resistivity is mainly determined by the terms $(n_h\mu_h^2 - n_e\mu_e^2)B$ and $(n_h - n_e)\mu_e^2\mu_h^2B^3$ at relatively low and high field, respectively. Therefore, the sign of Hall resistivity at high enough field will change when the dominate carrier type varies.

In-situ tuning of carrier concentration across the compensation point enables us to establish a direct and explicit relation between the large MR and the charge compensation. We extracted the MR values at $B = 14$ T and calculated the ratio of carrier densities (n_e/n_h) at different gate voltages, with results shown in Figure 2f. When V_{tg} changes from -10 V to 6 V, the ratio n_e/n_h increases monotonically from 0.87 to 1.39. In particular, the MR - V_{tg} curve shows a non-monotonic feature and reaches the maximum at the charge compensation point where $n_e/n_h=1$. The MR value decreases rapidly when carrier concentration slightly deviates from the perfect charge

compensation point. As the carrier mobility changes during the gate tuning process (Figure 2d), we also compared the gate dependence of $\mu_e\mu_h$ with the MR - V_{ig} curve (see Supporting Information). With the opposite gate dependence of electron and hole mobilities, the change of $\mu_e\mu_h$ is small and its varying trend is also inconsistent with the variation of MR, indicating that the carrier mobility is not the origin of the unusual change of MR. Moreover, the large MR value ($\sim 10600\%$) in our thin film (about 10 nm in thick) is about one to two orders of magnitude larger than previous reported values in samples with similar film thickness^{24, 28-34, 36}. Even, this value is also much larger than that in thicker films with higher mobility^{33, 36}. It is the perfect charge compensation that gives rise to the large MR in our thin film, which has never been achieved in thin film devices. In addition, we also observed the non-saturated increase of MR(B) curves near the charge compensation point, but the increasing rate of MR(B) becomes small at high field when n_e/n_h is far away from 1 (as shown in Supporting Information). These results unambiguously demonstrate that the charge compensation is the dominate physical origin of the large non-saturating MR in WTe₂.

Another important feature of the MR in WTe₂ can be manifested by its strong dependence on temperature. This behavior has been proposed to arise from the temperature-dependent electronic band structure of WTe₂^{15, 43, 48}. However, recent works^{49, 50} have shown that the temperature has a negligible effect on the band structure of WTe₂. The achieved charge compensation in our samples also allows us to explicitly study the effect of temperature on the MR and carrier dynamics. We carried out measurements of the MR and the Hall resistivity at different temperatures with $V_{\text{ig}} = -6$ V. As shown in Figure 3a, increasing temperature leads to the suppression of MR and a transition from nonlinear to quasi-linear curves of the Hall resistivity. We extracted the MR values at different magnetic fields and presented them as a function of temperature, as shown in Figure 3b. Noticeably, the MR(T) curves show similar tendency under different magnetic fields. The MR becomes saturated at low temperatures but dramatically decreases when $T > 10$ K. This is distinct from the field dependent turn-on behavior of the resistivity curves shown in Figure 1b, which further indicates that the MR(T) curves reflect the intrinsic characteristic of the magneto-

transport properties in WTe₂ instead of the turn-on behavior of $\rho(T)$ curves^{42, 43}.

We further employed two-band theory to analyze the experimental data shown in Figure 3a (see the fitting results in the Supporting Information). The extracted carrier density and mobility at different temperatures are presented in Figure 3c and Figure 3d, respectively. We found that both electron and hole concentrations increase slightly at low temperatures but always keep a nearly-perfect charge compensation for $T \leq 50$ K (inset of Figure 3c). At higher temperatures, an opposite variation behavior of electron and hole concentrations was observed, suggesting a thermal excitation induced change of Fermi surface⁴⁸. Different from the variation of electron and hole densities, the temperature dependence of electron mobility is similar to hole mobility. They are nearly independent of temperature below 10 K and start to decrease above 10 K. This temperature dependent behavior is similar to the tendency of MR(T) curves in Figure 3b.

By keeping charge-compensation over a wide temperature range, it is helpful for revealing the underlying physics of the temperature dependent magneto-transport. Under the condition of charge compensation, the Eq. (3) can be reduced to $MR(T) = \mu_e(T)\mu_h(T)B^2$, thus the temperature dependence of the MR is determined only by the change of the mobility under a magnetic field. With $T < 50$ K, we observed the similar temperature dependent variation of the MR and the mobility, which is consistent with the theory and further implies the same scattering mechanism behind these two different physics behaviors. At $10 \text{ K} < T < 50 \text{ K}$, the mobility is well fitted by $\mu \propto T^{-n}$ with $n = 1.23$ and 1.2 for electron and hole respectively, which suggests that the electron-phonon interactions dominate the scattering process within this temperature range⁵¹. Over the same temperature range, we fitted the temperature dependence of the MR at $B = 14 \text{ T}$ by using the equation $MR(T) \propto (a+bT^{-m})^2$, where a , b and m are free parameters. The extracted parameter m is 1.22, close to the obtained values of n for the mobility. This suggests that the dramatic decrease in the MR could be attributed to the electron-phonon scattering mechanism. At low temperatures ($T < 10 \text{ K}$), the MR tends to saturate, which is also observed at other gate voltages (Supporting Information). Note that similar

saturation behavior has also been reported in bulk WTe_2 , but the physical origins remain unclear. In our samples, the temperature dependent mobility curves exhibit same plateau at $T < 10$ K, indicating that the charge scattering mechanism dominates the magneto-transport. Together with the evidence that electron-electron (e-e) interactions are at play at low temperatures in the Figure 1b, we deduce that the e-e interactions may be the dominant scattering source that leads to the plateau of the MR and the mobility in WTe_2 and the impurity scattering at low temperature may play a role. Besides, at $T > 100$ K, both electron-phonon scattering and thermal excitation induced Fermi surface change account for the change in the MR. These results may be helpful for understanding the temperature magneto-transport in other materials with large MR⁵²⁻⁵⁷ like MoTe_2 , LaSb , WP_2 , PtBi_2 , etc.

In conclusion, we studied the physical origin of the large non-saturating MR in WTe_2 based on the high-quality thin film device. Through an electrostatic tuning approach, we achieved an *in-situ* tuning of charge carriers across the charge compensation point for the first time. The observed maximum MR with a record-high value ($\sim 10600\%$) at the charge compensation point offers a direct evidence for the charge compensation induced large non-saturating MR in the WTe_2 . By keeping the charge compensation over a wide temperature range, we clearly identified the close relation between temperature dependent MR and mobility, which further reveals the charge scattering mechanisms responsible for temperature dependence of magneto-transport. Our work opens up an avenue for achieving the large MR in the non-magnetic materials with electron-hole pockets and pave the way towards realization of nanostructure magnetic sensor and memory devices.

Growth of single crystals

The high quality single crystals of WTe_2 were grown by using high-temperature self-flux method. Both tungsten powders (99.9%) and tellurium pieces (99.999%) with ratio of 1:30 were placed into alumina crucibles in a glovebox full of inert gas, and sealed in quartz tubes under high vacuum. The tubes were heated and maintained at 1373 K for 10 h and then cooled down to 923 K slowly with a rate of 2 K/h. The tungsten flux was

separated in a centrifuge at 923 K.

Electrical measurement

The thin film device was measured in the Oxford cryostat with magnetic field up to 14 Tesla and a base temperature of about 1.6 K. The resistance was measured by using low-frequency Lock-in amplifier.

ASSOCIATED CONTENT

Supporting information

The Supporting information is available free of charge on the ACS Publications website at <http://pubs.acs.org>.

Effect of carriers' mobilities on the gate tunable magnetoresistance; the effect of the ratio of carrier density on the MR; two-band theory analysis of the magnetoresistance and the Hall resistivity curves at different temperatures; temperature-dependence of the magnetoresistance at different gate voltages; contact resistance of the film device at 1.6 K.

AUTHOR INFORMATION

Corresponding Authors

* E-mail: sjliang@nju.edu.cn.

* E-mail: miao@nju.edu.cn. Tel: +86-025-83621497. Fax: +86-025-83621497.

ORCID

Feng Miao: [0000-0002-1910-9781](https://orcid.org/0000-0002-1910-9781)

Bin Cheng: [0000-0002-2932-4370](https://orcid.org/0000-0002-2932-4370)

Kenji Watanabe: [0000-0003-3701-8119](https://orcid.org/0000-0003-3701-8119)

Author Contributions

^{||}Y.W. and L.W. contribute equally to this work.

Notes

The authors declare no competing financial interest.

Acknowledgements

This work was supported in part by the National Key Basic Research Program of China (2015CB921600), the National Natural Science Foundation of China (61625402, 61574076, 11774399), the Collaborative Innovation Center of Advanced Microstructures, Natural Science Foundation of Jiangsu Province (BK20180330 and BK20150055), Fundamental Research Funds for the Central Universities (020414380122, 020414380084), Beijing Natural Science Foundation (Z180008) and the program A/B for Outstanding PhD candidate of Nanjing University(201801A002). K.W. and T.T. acknowledge support from the Elemental Strategy Initiative conducted by the MEXT, Japan, A3 Foresight by JSPS and the CREST (JPMJCR15F3), JST.

Figures

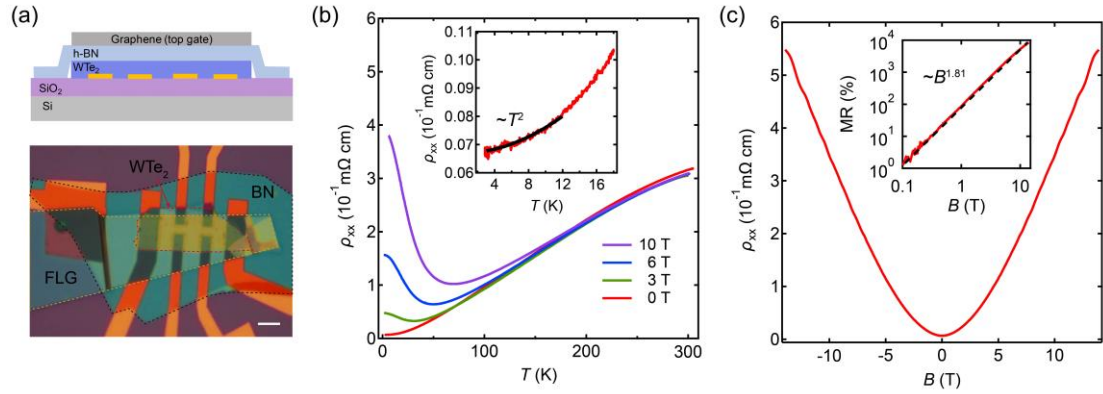


Figure 1. Characterization of the thin film device with h-BN as protective layer. (a) Optical image of 10 nm thick WTe₂ device, the boundary of the WTe₂ film is indicated by the red dashed line. The edges of few-layer graphene and h-BN are indicated by the yellow and black dashed lines, respectively. The length of the white scale bar is 5 μ m. The upper panel is the cross-sectional schematic structure of the device. (b) Temperature dependence of resistivity at $V_{tg} = -6$ V for different magnetic fields. The zero-field $\rho(T)$ curve at low temperature range is fitted by $\rho_{xx}(T) = \rho_0 + aT^2$ (solid black line in the inset). (c) Resistivity versus magnetic field $\rho(B)$ at 1.6 K ($V_{tg} = 0$ V), the inset shows the fitted result (dashed black line) of the magnetoresistance, which follows $MR \sim B^{1.81}$.

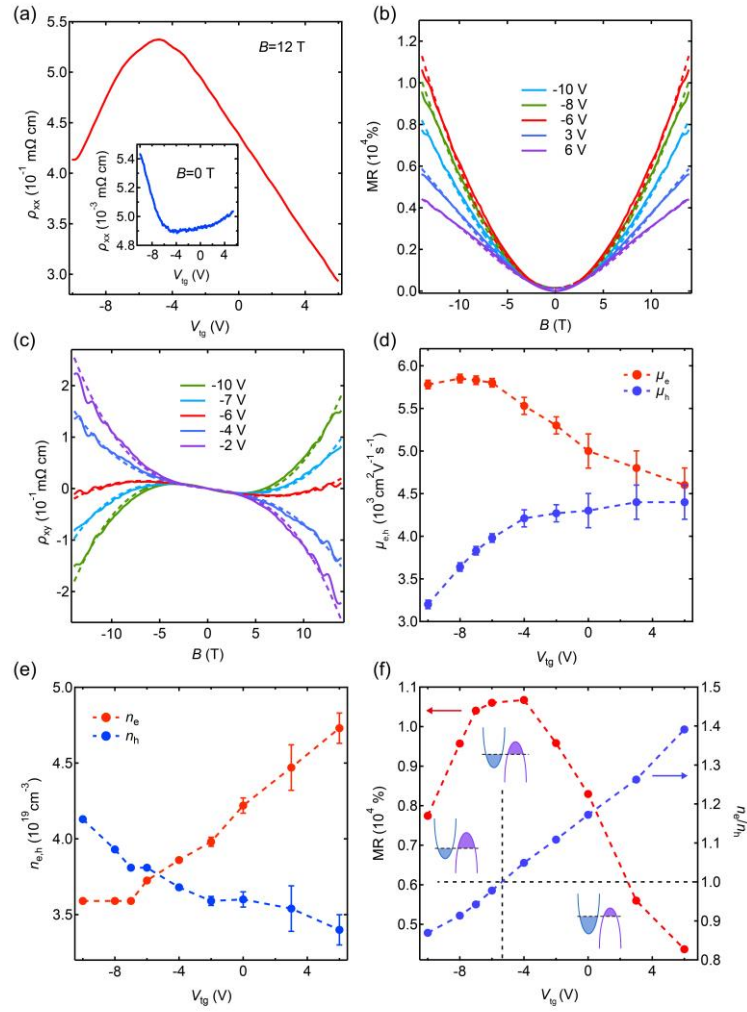


Figure 2. Gate-tunable magneto-transport of thin film device at 1.6 K. (a) Gate tunable resistivity with (main panel) and without (inset) magnetic field. (b) and (c) show the gate tunable MR and Hall resistivity curves, respectively. The two-band theory (dashed lines) has been used to fit the MR and Hall resistivity. (d) and (e) are the gate voltage dependence of the extracted mobility and carrier density respectively. The dominant carrier type is distinct at two sides of the crossover point on (e). (f) Comparison of the gate voltage dependent MR and carrier densities ratio. The MR curve reaches the maximum with tuning the carrier concentration through the charge compensation point ($n_e/n_h = 1$). The three schematic bands represent different scenarios for charge distribution in electron (blue) and hole (purple) pockets at different gate voltage ranges.

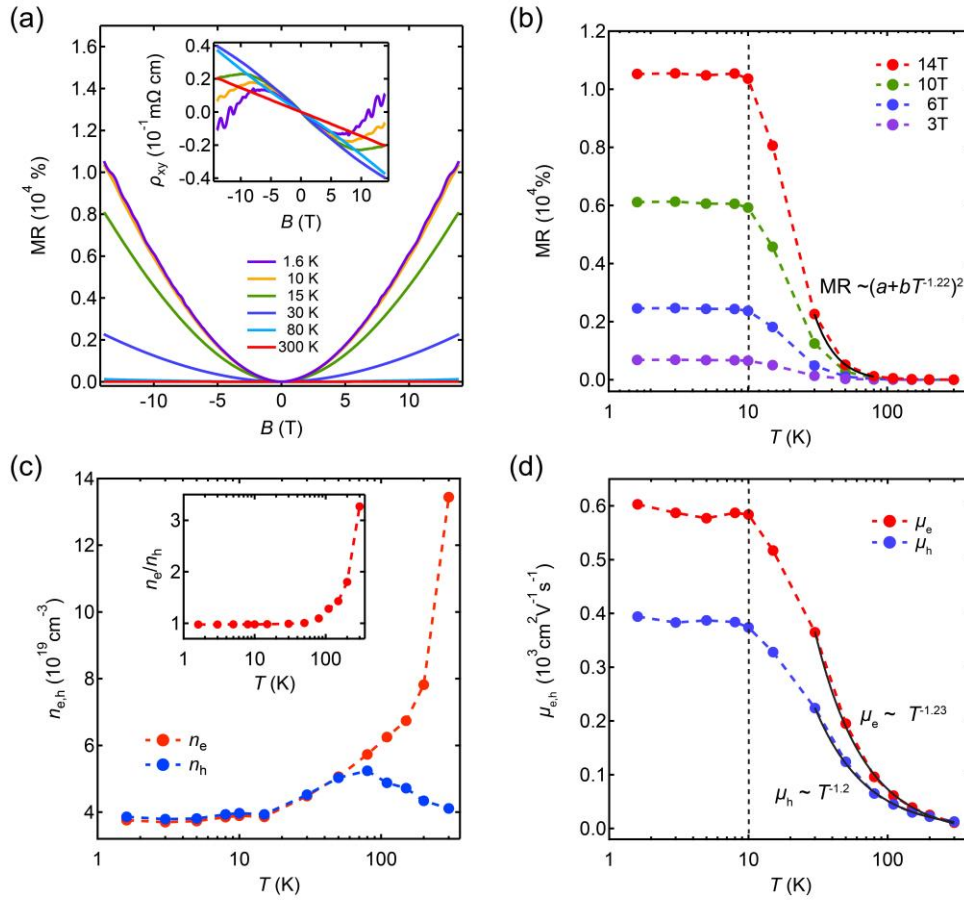


Figure 3. Analysis of temperature dependent magneto-transport at $V_{\text{tg}} = -6$ V. (a) $\text{MR}(B)$ versus magnetic field at different temperatures, the inset shows the corresponding Hall resistivity curves. (b) Temperature dependence of the MR at different magnetic fields. The decrease of $\text{MR}(T)$ follows $\sim (a + bT^{-1.22})^2$ (the solid black line). (c) Extracted carrier (electron and hole) densities as a function of temperature, the inset is the ratio of corresponding electron and hole densities. (d) Temperature dependence of mobilities for electron and hole densities. Power law (solid black lines) has been used to fit the experimental data (symbols).

References:

- (1). Ali, M. N.; Xiong, J.; Flynn, S.; Tao, J.; Gibson, Q. D.; Schoop, L. M.; Liang, T.; Haldolaarachchige, N.; Hirschberger, M.; Ong, N. P.; Cava, R. J. Large, non-saturating magnetoresistance in WTe_2 . *Nature* **2014**, 514, 205-208.
- (2). Lv, Y.; Li, X.; Zhang, B.; Deng, W. Y.; Yao, S.; Chen, Y. B.; Zhou, J.; Zhang, S.; Lu, M.; Zhang, L.; Tian, M.; Sheng, L.; Chen, Y. Experimental Observation of Anisotropic Adler-Bell-Jackiw Anomaly

in Type-II Weyl Semimetal $\text{WTe}_{1.98}$. Crystals at the Quasiclassical Regime. *Phys. Rev. Lett.* **2017**, 118, 096603.

(3). Soluyanov, A. A.; Gresch, D.; Wang, Z.; Wu, Q.; Troyer, M.; Dai, X.; Bernevig, B. A. Type-II Weyl semimetals. *Nature* **2015**, 527, 495-498.

(4). Wang, Y.; Liu, E.; Liu, H.; Pan, Y.; Zhang, L.; Zeng, J.; Fu, Y.; Wang, M.; Xu, K.; Huang, Z.; Wang, Z.; Lu, H.; Xing, D.; Wang, B.; Wan, X.; Miao, F. Gate-tunable negative longitudinal magnetoresistance in the predicted type-II Weyl semimetal WTe_2 . *Nat. Commun.* **2016**, 7, 13142.

(5). Fatemi, V.; Wu, S.; Cao, Y.; Bretheau, L.; Gibson, Q. D.; Watanabe, K.; Taniguchi, T.; Cava, R. J.; Jarillo-Herrero, P. Electrically tunable low-density superconductivity in a monolayer topological insulator. *Science* **2018**, 362, 926-929.

(6). Kang, D.; Zhou, Y.; Yi, W.; Yang, C.; Guo, J.; Shi, Y.; Zhang, S.; Wang, Z.; Zhang, C.; Jiang, S.; Li, A.; Yang, K.; Wu, Q.; Zhang, G.; Sun, L.; Zhao, Z. Superconductivity emerging from a suppressed large magnetoresistant state in tungsten ditelluride. *Nat. Commun.* **2015**, 6, 7804.

(7). Li, Q.; He, C.; Wang, Y.; Liu, E.; Wang, M.; Wang, Y.; Zeng, J.; Ma, Z.; Cao, T.; Yi, C.; Wang, N.; Watanabe, K.; Taniguchi, T.; Shao, L.; Shi, Y.; Chen, X.; Liang, S.; Wang, Q.; Miao, F. Proximity-Induced Superconductivity with Subgap Anomaly in Type II Weyl Semi-Metal WTe_2 . *Nano Lett.* **2018**, 18, 7962-7968.

(8). Pan, X.; Chen, X.; Liu, H.; Feng, Y.; Wei, Z.; Zhou, Y.; Chi, Z.; Pi, L.; Yen, F.; Song, F.; Wan, X.; Yang, Z.; Wang, B.; Wang, G.; Zhang, Y. Pressure-driven dome-shaped superconductivity and electronic structural evolution in tungsten ditelluride. *Nat. Commun.* **2015**, 6, 7805.

(9). Sajadi, E.; Palomaki, T.; Fei, Z.; Zhao, W.; Bement, P.; Olsen, C.; Luescher, S.; Xu, X.; Folk, J. A.; Cobden, D. H. Gate-induced superconductivity in a monolayer topological insulator. *Science* **2018**, 362, 922-925.

(10). Zhu, L.; Li, Q.; Lv, Y.; Li, S.; Zhu, X.; Jia, Z.; Chen, Y. B.; Wen, J.; Li, S. Superconductivity in Potassium-Intercalated $\text{T}_d\text{-WTe}_2$. *Nano Lett.* **2018**, 18, 6585-6590.

(11). Fei, Z.; Zhao, W.; Palomaki, T. A.; Sun, B.; Miller, M. K.; Zhao, Z.; Yan, J.; Xu, X.; Cobden, D. H. Ferroelectric switching of a two-dimensional metal. *Nature* **2018**, 560, 336-339.

(12). Wu, S.; Fatemi, V.; Gibson, Q. D.; Watanabe, K.; Taniguchi, T.; Cava, R. J.; Jarillo-Herrero, P. Observation of the quantum spin Hall effect up to 100 kelvin in a monolayer crystal. *Science* **2018**, 359, 76-79.

(13). Luo, Y.; Li, H.; Dai, Y. M.; Miao, H.; Shi, Y. G.; Ding, H.; Taylor, A. J.; Yarotski, D. A.; Prasankumar, R. P.; Thompson, J. D. Hall effect in the extremely large magnetoresistance semimetal WTe_2 . *Appl. Phys. Lett.* **2015**, 107, 182411.

(14). Pan, X.; Pan, Y.; Jiang, J.; Zuo, H.; Liu, H.; Chen, X.; Wei, Z.; Zhang, S.; Wang, Z.; Wan, X.; Yang, Z.; Feng, D.; Xia, Z.; Li, L.; Song, F.; Wang, B.; Zhang, Y.; Wang, G. Carrier balance and linear magnetoresistance in type-II Weyl semimetal WTe_2 . *Front. Phys.* **2017**, 12, 127203.

(15). Pletikosic, I.; Ali, M. N.; Fedorov, A. V.; Cava, R. J.; Valla, T. Electronic structure basis for the extraordinary magnetoresistance in WTe_2 . *Phys. Rev. Lett.* **2014**, 113, 216601.

(16). Feng, B.; Chan, Y.; Feng, Y.; Liu, R.; Chou, M.; Kuroda, K.; Yaji, K.; Harasawa, A.; Moras, P.; Barinov, A.; Malaeb, W.; Bareille, C.; Kondo, T.; Shin, S.; Komori, F.; Chiang, T.; Shi, Y.; Matsuda, I. Spin texture in type-II Weyl semimetal WTe_2 . *Phys. Rev. B* **2016**, 94, 195134.

(17). Jiang, J.; Tang, F.; Pan, X. C.; Liu, H. M.; Niu, X. H.; Wang, Y. X.; Xu, D. F.; Yang, H. F.; Xie, B. P.; Song, F. Q.; Dudin, P.; Kim, T. K.; Hoesch, M.; Das, P. K.; Vobornik, I.; Wan, X. G.; Feng, D. L. Signature of Strong Spin-Orbital Coupling in the Large Nonsaturating Magnetoresistance Material WTe_2 .

Phys. Rev. Lett. **2015**, 115, 166601.

(18). Caputo, M.; Khalil, L.; Papalazarou, E.; Nilforoushan, N.; Perfetti, L.; Taleb-Ibrahimi, A.; Gibson, Q. D.; Cava, R. J.; Marsi, M. Dynamics of out-of-equilibrium electron and hole pockets in the type-II Weyl semimetal candidate WTe₂. *Phys. Rev. B* **2018**, 97, 115115.

(19). Das, P. K.; Di Sante, D.; Vobornik, I.; Fujii, J.; Okuda, T.; Bruyer, E.; Gyenis, A.; Feldman, B. E.; Tao, J.; Ciancio, R.; Rossi, G.; Ali, M. N.; Picozzi, S.; Yadzani, A.; Panaccione, G.; Cava, R. J. Layer-dependent quantum cooperation of electron and hole states in the anomalous semimetal WTe₂. *Nat. Commun.* **2016**, 7, 10847.

(20). Di Sante, D.; Das, P. K.; Bigi, C.; Ergönenc, Z.; Gürtler, N.; Krieger, J. A.; Schmitt, T.; Ali, M. N.; Rossi, G.; Thomale, R.; Franchini, C.; Picozzi, S.; Fujii, J.; Strocov, V. N.; Sangiovanni, G.; Vobornik, I.; Cava, R. J.; Panaccione, G. Three-Dimensional Electronic Structure of the Type-II Weyl Semimetal WTe₂. *Phys. Rev. Lett.* **2017**, 119, 026403.

(21). Cai, P. L.; Hu, J.; He, L. P.; Pan, J.; Hong, X. C.; Zhang, Z.; Zhang, J.; Wei, J.; Mao, Z. Q.; Li, S. Y. Drastic Pressure Effect on the Extremely Large Magnetoresistance in WTe₂: Quantum Oscillation Study. *Phys. Rev. Lett.* **2015**, 115, 057202.

(22). Fu, D.; Pan, X.; Bai, Z.; Fei, F.; Umana-Membreno, G.; Song, H.; Wang, X.; Wang, B.; Song, F. Tuning the electrical transport of type II Weyl semimetal WTe₂ nanodevices by Mo doping. *Nanotechnology* **2018**, 29, 135705.

(23). Lv, Y.; Zhang, B.; Li, X.; Pang, B.; Zhang, F.; Lin, D.; Zhou, J.; Yao, S.; Chen, Y. B.; Zhang, S.; Lu, M.; Liu, Z.; Chen, Y.; Chen, Y. Dramatically decreased magnetoresistance in non-stoichiometric WTe₂ crystals. *Sci. Rep.* **2016**, 6, 26903.

(24). Liu, X.; Zhang, Z.; Cai, C.; Tian, S.; Kushwaha, S.; Lu, H.; Taniguchi, T.; Watanabe, K.; Cava, R. J.; Jia, S.; Chen, J. Gate tunable magneto-resistance of ultra-thin WTe₂ devices. *2D Mater.* **2017**, 4, 021018.

(25). Ali, M. N.; Schoop, L.; Xiong, J.; Flynn, S.; Gibson, Q.; Hirschberger, M.; Ong, N. P.; Cava, R. J. Correlation of crystal quality and extreme magnetoresistance of WTe₂. *EPL (Europhysics Letters)* **2015**, 110, 67002.

(26). Fatemi, V.; Gibson, Q. D.; Watanabe, K.; Taniguchi, T.; Cava, R. J.; Jarillo-Herrero, P. Magnetoresistance and quantum oscillations of an electrostatically tuned semimetal-to-metal transition in ultrathin WTe₂. *Phys. Rev. B* **2017**, 95, 041410(R).

(27). Gong, J.; Yang, J.; Ge, M.; Wang, Y.; Liang, D.; Luo, L.; Yan, X.; Zhen, W.; Weng, S.; Pi, L.; Zhang, C.; Zhu, W. Non-Stoichiometry Effects on the Extreme Magnetoresistance in Weyl Semimetal WTe₂. *Chin. Phys. Lett.* **2018**, 35, 97101.

(28). Luo, X.; Fang, C.; Wan, C.; Cai, J.; Liu, Y.; Han, X.; Lu, Z.; Shi, W.; Xiong, R.; Zeng, Z. Magnetoresistance and Hall resistivity of semimetal WTe₂ ultrathin flakes. *Nanotechnology* **2017**, 28, 145704.

(29). Na, J.; Hoyer, A.; Schoop, L.; Weber, D.; Lotsch, B. V.; Burghard, M.; Kern, K. Tuning the magnetoresistance of ultrathin WTe₂ sheets by electrostatic gating. *Nanoscale* **2016**, 8, 18703-18709.

(30). Wang, L.; Gutiérrez-Lezama, I.; Barreteau, C.; Ki, D.; Giannini, E.; Morpurgo, A. F. Direct Observation of a Long-Range Field Effect from Gate Tuning of Nonlocal Conductivity. *Phys. Rev. Lett.* **2016**, 117, 176601.

(31). Wang, L.; Gutiérrez-Lezama, I.; Barreteau, C.; Ubrig, N.; Giannini, E.; Morpurgo, A. F. Tuning magnetotransport in a compensated semimetal at the atomic scale. *Nat. Commun.* **2015**, 6, 8892.

(32). Wang, Y.; Wang, K.; Reutt-Robey, J.; Paglione, J.; Fuhrer, M. S. Breakdown of compensation and

- persistence of nonsaturating magnetoresistance in gated WTe₂ thin flakes. *Phys. Rev. B* **2016**, 93, 121108(R).
- (33). Woods, J. M.; Shen, J.; Kumaravadivel, P.; Pang, Y.; Xie, Y.; Pan, G. A.; Li, M.; Altman, E. I.; Lu, L.; Cha, J. J. Suppression of Magnetoresistance in Thin WTe₂ Flakes by Surface Oxidation. *ACS Appl. Mater. Inter.* **2017**, 9, 23175-23180.
- (34). Xiang, F.; Srinivasan, A.; Du, Z. Z.; Klochan, O.; Dou, S.; Hamilton, A. R.; Wang, X. Thickness-dependent electronic structure in WTe₂ thin films. *Phys. Rev. B* **2018**, 98, 035115.
- (35). Ye, F.; Lee, J.; Hu, J.; Mao, Z.; Wei, J.; Feng, P. X. L. Environmental Instability and Degradation of Single- and Few-Layer WTe₂ Nanosheets in Ambient Conditions. *Small* **2016**, 12, 5802-5808.
- (36). Yi, Y.; Wu, C.; Wang, H.; Liu, H.; Li, H.; Zhang, H.; He, H.; Wang, J. Thickness dependent magneto transport properties of WTe₂ thin films. *Solid State Commun.* **2017**, 260, 45-49.
- (37). Rana, K. G.; Dejene, F. K.; Kumar, N.; Rajamathi, C. R.; Sklarek, K.; Felser, C.; Parkin, S. S. P. Thermopower and Unconventional Nernst Effect in the Predicted Type-II Weyl Semimetal WTe₂. *Nano Lett.* **2018**, 18, 6591-6596.
- (38). Zhang, E.; Chen, R.; Huang, C.; Yu, J.; Zhang, K.; Wang, W.; Liu, S.; Ling, J.; Wan, X.; Lu, H.; Xiu, F. Tunable Positive to Negative Magnetoresistance in Atomically Thin WTe₂. *Nano Lett.* **2017**, 17, 878-885.
- (39). Li, J.; Cheng, S.; Liu, Z.; Zhang, W.; Chang, H. Centimeter-Scale, Large-Area, Few-Layer 1T' - WTe₂ Films by Chemical Vapor Deposition and Its Long-Term Stability in Ambient Condition. *The Journal of Physical Chemistry C* **2018**, 122, 7005-7012.
- (40). Mleccko, M. J.; Xu, R. L.; Okabe, K.; Kuo, H.; Fisher, I. R.; Wong, H. S. P.; Nishi, Y.; Pop, E. High Current Density and Low Thermal Conductivity of Atomically Thin Semimetallic WTe₂. *ACS Nano* **2016**, 10, 7507-7514.
- (41). Wang, L.; Meric, I.; Huang, P. Y.; Gao, Q.; Gao, Y.; Tran, H.; Taniguchi, T.; Watanabe, K.; Campos, L. M.; Muller, D. A.; Guo, J.; Kim, P.; Hone, J.; Shepard, K. L.; Dean, C. R. One-dimensional electrical contact to a two-dimensional material. *Science* **2013**, 342, 614-617.
- (42). Wang, Y. L.; Thoutam, L. R.; Xiao, Z. L.; Hu, J.; Das, S.; Mao, Z. Q.; Wei, J.; Divan, R.; Luican-Mayer, A.; Crabtree, G. W.; Kwok, W. K. Origin of the turn-on temperature behavior in WTe₂. *Phys. Rev. B* **2015**, 92, 180402(R).
- (43). Thoutam, L. R.; Wang, Y. L.; Xiao, Z. L.; Das, S.; Luican-Mayer, A.; Divan, R.; Crabtree, G. W.; Kwok, W. K. Temperature-Dependent Three-Dimensional Anisotropy of the Magnetoresistance in WTe₂. *Phys. Rev. Lett.* **2015**, 115, 046602.
- (44). Zhao, Y.; Liu, H.; Yan, J.; An, W.; Liu, J.; Zhang, X.; Wang, H.; Liu, Y.; Jiang, H.; Li, Q.; Wang, Y.; Li, X.; Mandrus, D.; Xie, X. C.; Pan, M.; Wang, J. Anisotropic magnetotransport and exotic longitudinal linear magnetoresistance in WTe₂ crystals. *Phys. Rev. B* **2015**, 92, 041104(R).
- (45). Rhodes, D.; Das, S.; Zhang, Q. R.; Zeng, B.; Pradhan, N. R.; Kikugawa, N.; Manousakis, E.; Balicas, L. Role of spin-orbit coupling and evolution of the electronic structure of WTe₂ under an external magnetic field. *Phys. Rev. B* **2015**, 92, 125152.
- (46). Zhu, Z.; Lin, X.; Liu, J.; Fauqué, B.; Tao, Q.; Yang, C.; Shi, Y.; Behnia, K. Quantum Oscillations, Thermoelectric Coefficients, and the Fermi Surface of Semimetallic WTe₂. *Phys. Rev. Lett.* **2015**, 114, 176601.
- (47). Sondheimer, E. H.; Wilson, A. H. The theory of the magneto-resistance effects in metals. *Proc. R. Soc. London Series A Math. Phys. Sci.* **1947**, 190, 435-455.
- (48). Wu, Y.; Jo, N. H.; Ochi, M.; Huang, L.; Mou, D.; Bud'Ko, S. L.; Canfield, P. C.; Trivedi, N.; Arita,

- R.; Kaminski, A. Temperature-Induced Lifshitz Transition in WTe_2 . *Phys. Rev. Lett.* **2015**, 115, 166602.
- (49). Liu, G.; Liu, H.; Zhou, J.; Wan, X. Temperature effect on lattice and electronic structures of WTe_2 from first-principles study. *J. Appl. Phys.* **2017**, 121, 045104.
- (50). Thirupathaiyah, S.; Jha, R.; Pal, B.; Matias, J. S.; Das, P. K.; Vobornik, I.; Ribeiro, R. A.; Sarma, D. D. Temperature-independent band structure of WTe_2 as observed from angle-resolved photoemission spectroscopy. *Phys. Rev. B* **2017**, 96, 165149.
- (51). Kaasbjerg, K.; Thygesen, K. S.; Jacobsen, K. W. Phonon-limited mobility in n-type single-layer MoS_2 from first principles. *Phys. Rev. B* **2012**, 85, 115317.
- (52). Du, J.; Lou, Z.; Zhang, S.; Zhou, Y.; Xu, B.; Chen, Q.; Tang, Y.; Chen, S.; Chen, H.; Zhu, Q.; Wang, H.; Yang, J.; Wu, Q.; Yazyev, O. V.; Fang, M. Extremely large magnetoresistance in the topologically trivial semimetal α - WP_2 . *Phys. Rev. B* **2018**, 97, 245101.
- (53). Gao, W.; Hao, N.; Zheng, F.; Ning, W.; Wu, M.; Zhu, X.; Zheng, G.; Zhang, J.; Lu, J.; Zhang, H.; Xi, C.; Yang, J.; Du, H.; Zhang, P.; Zhang, Y.; Tian, M. Extremely Large Magnetoresistance in a Topological Semimetal Candidate Pyrite PtBi_2 . *Phys. Rev. Lett.* **2017**, 118, 256601.
- (54). Kumar, N.; Sun, Y.; Xu, N.; Manna, K.; Yao, M.; Süß, V.; Leermakers, I.; Young, O.; Förster, T.; Schmidt, M.; Borrmann, H.; Yan, B.; Zeitler, U.; Shi, M.; Felser, C.; Shekhar, C. Extremely high magnetoresistance and conductivity in the type-II Weyl semimetals WP_2 and MoP_2 . *Nat. Commun.* **2017**, 8, 1642.
- (55). Luo, X.; Xiao, R. C.; Chen, F. C.; Yan, J.; Pei, Q. L.; Sun, Y.; Lu, W. J.; Tong, P.; Sheng, Z. G.; Zhu, X. B.; Song, W. H.; Sun, Y. P. Origin of the extremely large magnetoresistance in topological semimetal PtSn_4 . *Phys. Rev. B* **2018**, 97, 205132.
- (56). Zhong, S.; Tiwari, A.; Nichols, G.; Chen, F.; Luo, X.; Sun, Y.; Tsen, A. W. Origin of magnetoresistance suppression in thin γ - MoTe_2 . *Phys. Rev. B* **2018**, 97, 241409(R).
- (57). Han, F.; Xu, J.; Botana, A. S.; Xiao, Z. L.; Wang, Y. L.; Yang, W. G.; Chung, D. Y.; Kanatzidis, M. G.; Norman, M. R.; Crabtree, G. W.; Kwok, W. K. Separation of electron and hole dynamics in the semimetal LaSb . *Phys. Rev. B* **2017**, 96, 125112.